Title
CORRECTION OF ATMOSPHERIC DISTORTION WITH AN IMAGE-SHARPENING TELESCOPE

Author
Buffington, A.

Publication Date
1976-02-01

Submitted to Applied Optics

LBL-4803
Preprint

CORRECTION OF ATMOSPHERIC DISTORTION WITH AN IMAGE-SHARPENING TELESCOPE

A. Buffington, F. S. Crawford, R. A. Muller,
A. J. Schwemin, and R. G. Smits

February 1976

Prepared for the U. S. Energy Research and
Development Administration under Contract W-7405-ENG-48

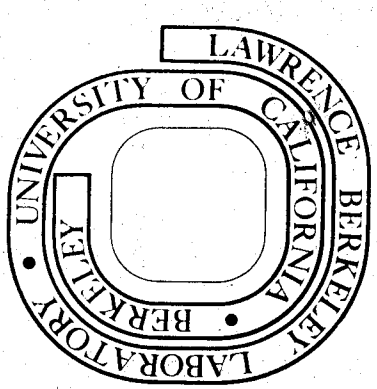

DISCLAIMER

CORRECTION OF ATMOSPHERIC DISTORTION WITH AN IMAGE-SHARPENING TELESCOPE

A. Buffington, F.S. Crawford, R.A. Muller,
A.J. Schwemin, and R.G. Smits

Lawrence Berkeley Laboratory and Space Sciences Laboratory
University of California, Berkeley, California 94720

ABSTRACT:

We have built and tested a 30 cm x 5 cm aperture telescope which uses six moveable mirrors to compensate for atmospherically induced phase distortion. A feedback system adjusts the mirrors in real time to maximize the intensity of light passing through a narrow slit in the image plane. We have achieved essentially diffraction-limited performance when imaging both laser and white-light objects through 250 meters of turbulent atmosphere. The behavior of our telescope was accurately predicted by computer simulations. The system has yet to achieve its full potential, but has already operated successfully for objects as dim as 5th magnitude.

I. INTRODUCTION

In a recent article[1], Muller and Buffington showed that certain image-plane sharpness functions, when evaluated for a system such as a large astronomical telescope, have their absolute maxima only when atmospheric or other phase perturbations have been removed. In addition, through the use of computer simulations, they showed that such sharpness functions providing feedback to a flexible mirror like that envisaged by Babcock[2] yield diffraction-limited telescope images in real time. Two such sharpness functions are given by

$$S_1 = \int dx\, dy\, I^2(x,y) \tag{1}$$

and

$$S_2 = \int dx\, dy\, I(x,y)\, M(x,y) \tag{2}$$

where x and y denote image plane coordinates, I(x,y) is the image-plane irradiance, and M(x,y) is a mask which is an estimate of the true restored image. S_1 restores the image of an arbitrary object distribution, but requires complicated image-plane data processing. S_2 is very simply carried out with a mask and a single photomultiplier, but may have difficulties if the correspondence between mask and true restored image is poor.

In this article, we describe the construction, calibration, and test of a small telescope system which demonstrates the practical application of image sharpening to produce corrected images in real time. Alternative systems to accomplish this goal are being developed at several laboratories,[3] including Itek, Perkin-Elmer, and Bell. A generalized framework for the analysis of such adaptive-optics systems has been developed by Dyson.[4] Our system has achieved

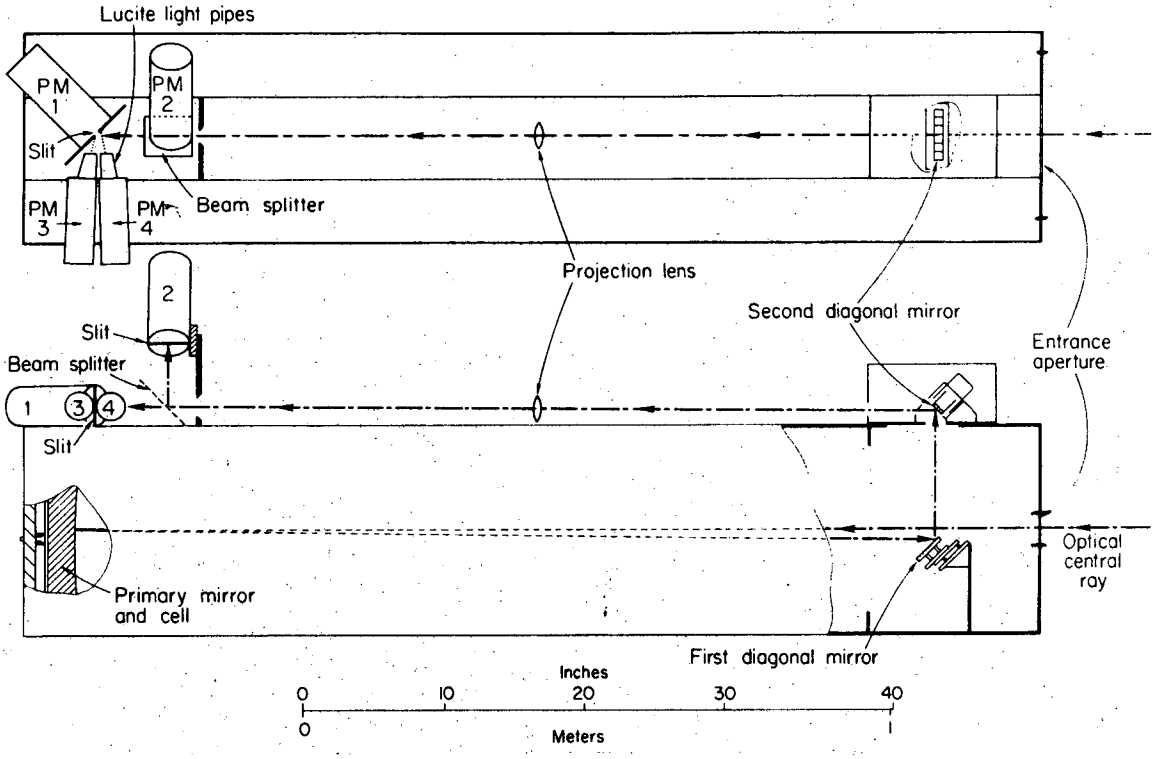

XBL 762-2246

Figure 1. Mechanical layout of the apparatus. Incident light passes through the entrance aperture, is focused by the primary mirror, reflects off the first and second diagonal mirrors, and comes to an image just in front of the projection lens. The first diagonal is mounted on piezoelectric columns which allow steering of the image in the dimension of good resolution. The second diagonal is made of six independent mirrors which can be moved perpendicular to the mirror plane. The projection lens re-focuses the image onto the slits in front of the photomultipliers PM-1 and PM-2. PM-1 measures the sharpness and is used to provide feedback to the six mirrors of the second diagonal. PM-2 and its slit are mechanically translated perpendicular to the beam lines and are used to record the image. PM-3 and PM-4 receive the light which does not pass through the slit for PM-1, and they are used to steer the first diagonal mirror to keep the image centered upon the sharpness slit. The telescope mount (not shown) allows rotation of the entire telescope about the axis of its barrel, thus permitting re-orientation of the direction of good resolution.

essentially diffraction-limited performance from a 30 cm x 5 cm aperture, imaging both white light and laser objects through 250 meters of turbulent atmosphere.

II. APPARATUS

A. GENERAL CONFIGURATION

The overall configuration of the telescope is shown in figure 1. The 30 cm diameter f/8 primary mirror is masked at the front of the telescope by an entrance aperture of 30 cm x 5 cm. This aperture minimizes the number of adjustable elements and yet gives a resolution fine enough to be capable of interesting astronomical measurements, such as the separation of double stars. When corrected, an aperture of this shape should have six times better resolution in one dimension than the other, thus producing essentially a one-dimensional image. Two diagonal mirrors bring the light to a lens which projects an enlarged image onto the sharpness slit with its photomultiplier PM-1. The six moveable optical elements which comprise the second diagonal mirror are driven by the control electronics. They maximize the signal from PM-1 and thus compensate the atmospheric phase distortions. A pair of steering photomultipliers (PM-3 and PM-4) provide the signal which drives the first diagonal to keep the image centered. The beam splitter directs 20% of the light to another photomultiplier (PM-2) which is used to scan the image in the high-resolution dimension; its output as a function of position is recorded on an X-Y plotter.

The system uses the sharpness function S_2 with a mask function $M(x,y)$ imposed by the slit in front of the photomultiplier PM-1. The

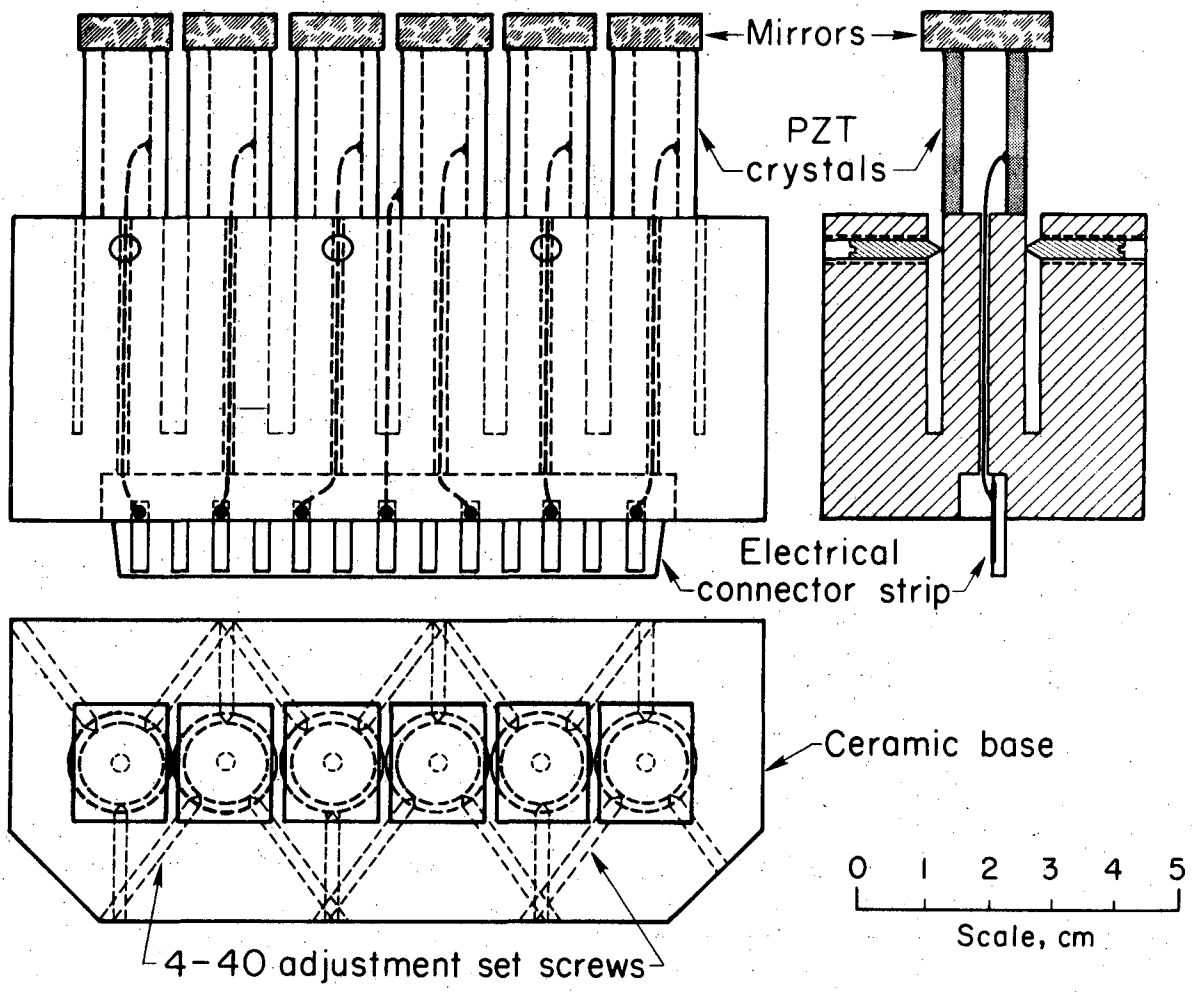

XBL 762-2272

Figure 2. Design for the flexible mirror. Mirror plane angles are adjusted by the set-screws, while the positions are adjusted by bias voltages placed on the piezoelectric crystals. Angles and mean mirror positions are fixed in the initial calibrations of the mirror, while rapid perturbations in mirror position about the mean perform the active wavefront phase correction.

slit width is somewhat less than a FWHM of the restored diffraction pattern at that location. The flexible optics consist of six mirrors driven by piezoelectric "crystals" acting as pistons. Computer simulations[1] have shown that this mask function and mirror arrangement should be sufficient to achieve essentially diffraction-limited performance when viewing an unresolved object.

B. MOVEABLE MIRRORS

The critical element of the image-sharpening system is the second diagonal mirror, containing the six moveable elements which correct the atmospheric phase distortion. Figures 2 and 3 show the construction of this "flexible mirror". Six pieces of glass 1.25 cm x 1.9 cm x 0.5 cm were selected for flatness. These were aluminized and placed in a row with 0.15 cm gaps between, in optical contact with a large flat. A ceramic base was prepared which had six mounting columns, each of which could be pushed by any of three set-screws to adjust the angles between column axes and the rear plane of the base. Six piezoelectric cylinders were glued onto the column ends, and the cylinder ends were lapped into a common plane after the glue had hardened. Finally, the assembly was glued with low expansion epoxy onto the six mirrors that had been placed on the optical flat. The eighteen adjustment screws could then be used, when the epoxy had hardened, to make the planes of the six individual mirrors parallel, and bias voltages on the piezoelectric cylinders could then make the six planes coincident. The piezoelectric cylinders move perpendicular to the plane of the mirrors, and fractional-wavelength mirror movements can be carried out by this system in as little as 0.06

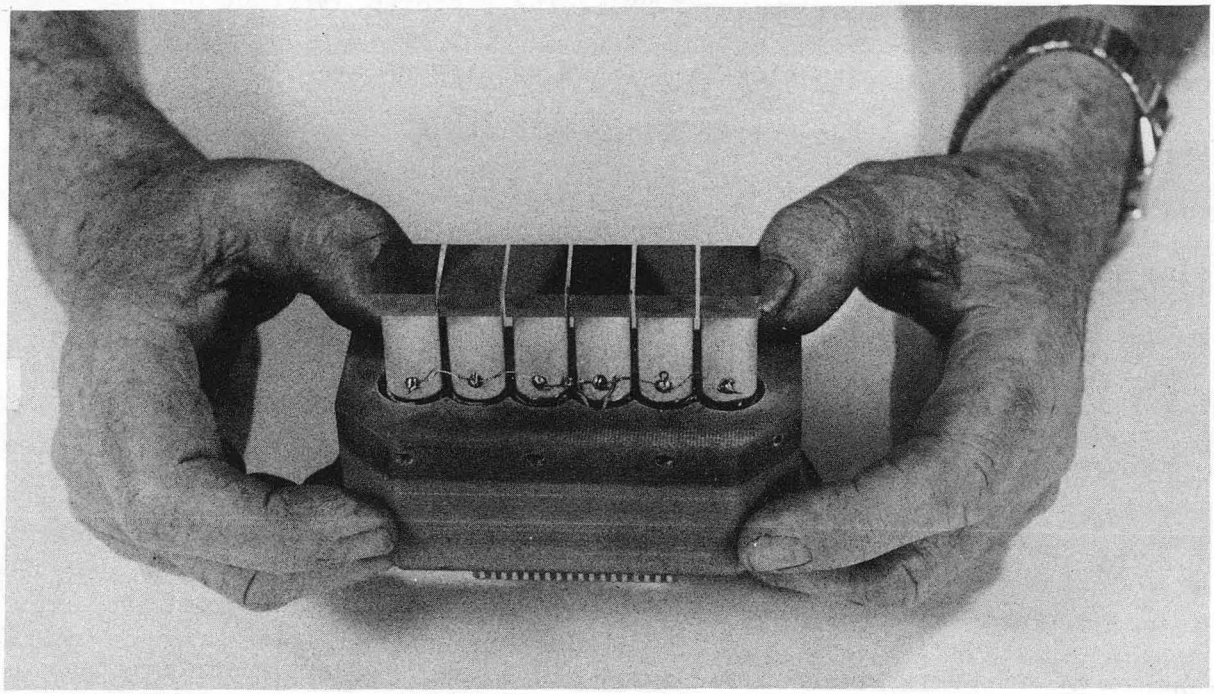

CBB 756-4230

Figure 3. Photograph of the flexible mirror. Mirrors, piezoelectric columns, and mounting base are visible, as are the access holes for half of the eighteen angle adjustment set-screws. The electrical connections to the mirror take place through the circuit-board strip just visible below the main mirror mounting base.

milliseconds. Application of ±1000 volts results in a motion of ±2.5 microns.

The first diagonal mirror, used to keep the image centered on the sharpness slit, was mounted on three other piezoelectric columns. These steer the image along the dimension of good resolution by ±10 arc sec with the application of ±1000 volts. This steering capability, although not necessary for the horizontal-path tests to be reported here, is vital to correct steering errors in the equatorial drive of astronomical telescopes. By removing first-order image translation directly, however, the steering does lessen the corrections that the second diagonal must provide, thus slightly improving the resultant diffraction pattern.

C. PHOTOMULTIPLIERS

The sharpness-measuring photomultiplier PM-1 receives the light which passes through a narrow slit in a mirror at the secondary focus. The remainder of this light is reflected into the two steering photomultipliers, PM-3 and PM-4, which measure the balance of the light on the two sides of the slit. The scanning photomultiplier PM-2 is used to record the image.

The quantum efficiencies of PM-1 and PM-2 were significantly enhanced by mounting them at 45° to the incoming light and using a prism[5] to introduce the light into the photomultiplier, as shown in figure 4. The light is trapped within the glass face of the photomultiplier, where it makes five encounters with the photoelectric surface rather than the usual single encounter. We were able to use this technique because the light is well collimated at the slit. For laser light at

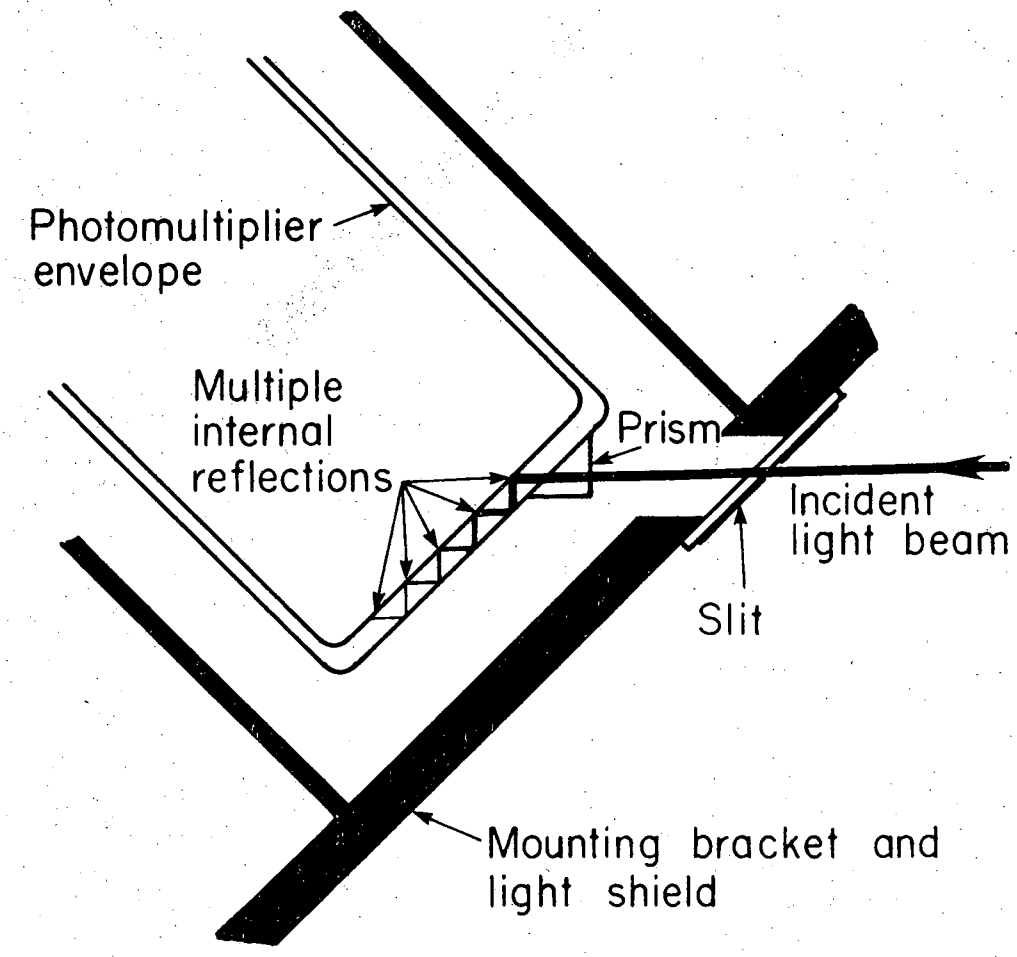

XBL 762-2247

Figure 4. Mounting of photomultipliers behind slits. The incident light is introduced into the face of the photomultiplier through a prism glued to the face. The light becomes trapped within the face, undergoing typically five reflective encounters with the photocathode before reaching the opposite side of the tube. The slit is made by evaporating aluminum onto a glass microscope slide except in a narrow line which was covered during the evaporation process.

6328Å and EMI 9558QB photomultipliers the enhancement was found to be a factor of four.

D. ELECTRONICS

Figure 5 shows a block diagram of the electronics. The control circuits introduced a small perturbation (typically 0.05 to 0.10 microns) into the position of each of the six moveable mirrors in sequence; if the "new" sharpness signal was larger than the "old" sharpness signal, the perturbation was left in place--otherwise the mirror was moved back. After one such cycle through the six mirrors, taking typically 4 ms, the sequence was repeated with perturbations in the other direction. A detailed sequence of program steps is given in Table I. Both the program logic and mirror logic blocks were built using standard TTL integrated circuit chips, together with programmable read-only memory chips (PROMs) to define the logic of Table I and the proper sequence of mirror motions.

Figure 5 also shows the arrangement for the telescope steering logic and for the data recording system. The light to the left and to the right of the sharpness-defining slit was picked up by lucite lightpipes and brought out to two RCA 6199 photomultipliers. The gains of these were matched. The steering logic then moved the first diagonal mirror to equalize the light into each photomultiplier, and thus to center the image on the sharpness-defining slit. The photomultiplier PM-2 and its slit were mounted on a mechanical slide whose position was encoded by the potentiometer P. The capacitor C integrated the PM-2 output with typically 2 sec time constant in order to give a smooth trace on the X-Y plotter as the slide was moved over its range.

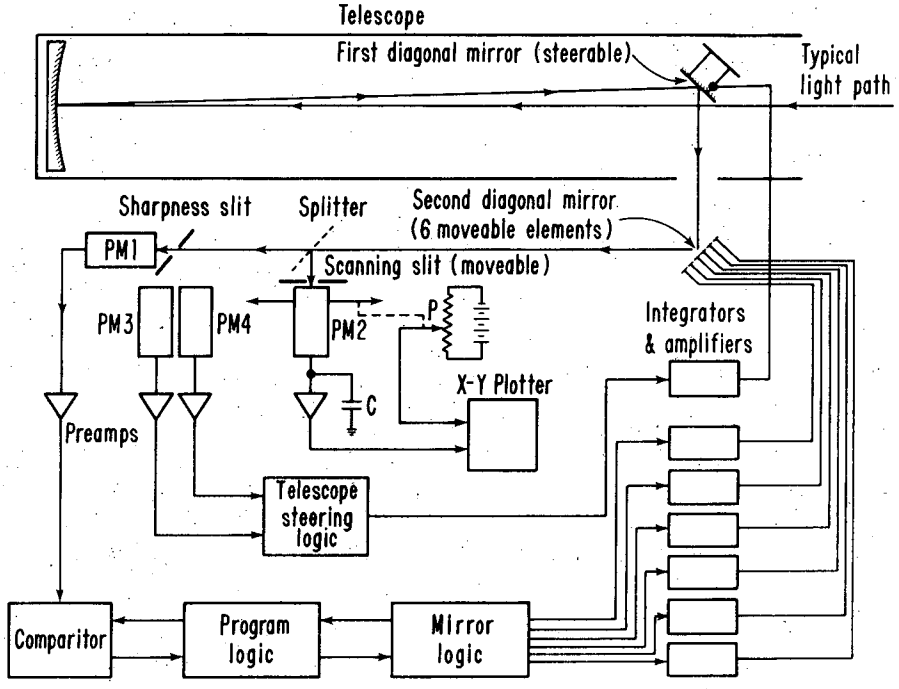

XBL 762-2245

Figure 5. Block diagram of the electronics. The incident light reflects off the first and second diagonal mirrors and then proceeds to the four photomultipliers. The sharpness slit with its photomultiplier PM-1 defines the desired image location and size. The beam splitter sends 20% of the light to the scanning photomultiplier PM-2 and its slit. These can be moved mechanically across the image plane to record the image. The potentiometer P encodes the position of the slit, and the output is integrated with typically several seconds integration time by the capacitor C. The X-Y plotter graphs the data. The steering photomultipliers PM-3 and PM-4 detect the light *not* passing through the sharpness slit and adjust the angle of the first diagonal mirror to center the image on the slit.

TABLE I. PROGRAM LOGIC FOR THE FLEXIBLE TELESCOPE SYSTEM

Step Number*	Instruction
1	Reset Mirror Logic Counter
2	Zero "New" Integrator
3	Integrate Sharpness PM into "New"
4	Load "New" into "Old"
5	Advance Mirror Logic Counter
6	Move Mirror
7	Zero "New" Integrator
8	Integrate Sharpness PM into "New"
9	If "New" less than "Old" go to step 13
10	Load "New" into "Old"
11	Advance Mirror Logic Counter
12	Go to step 15
13	Advance Mirror Logic Counter
14	Replace Mirror
15	If Mirror Logic Counter not finished, go to step 5
16	Go to Step 1

* The time inteval for each of these steps is 10 μ sec, except for the sharpness integrations, whose time is variable from 0.4 to 4 msec; and the mirror motion instructions which determine the size of the perturbations, whose time is variable from 0.06 to 0.6 msec.

E. SYSTEM ALIGNMENT

The system was aligned by using unresolvable light sources (laser or white light) placed 250 meters away from the laboratory window. The mechanical screw adjustments on each of the six moveable mirrors allowed us to tilt each of the mirrors until their Airy disks overlapped. Coincident Airy disks guarantee that the planes of the individual mirrors are parallel, or at least parallel to a spherical surface that can be corrected for by a slight focus adjustment with the projection lens. Because the mirrors had been pre-aligned by being pressed against an optical flat (section B), each mirror typically needed only a small screw adjustment of the order of the size of its Airy disk. To insure that the planes of the individual mirrors are coincident, and not just parallel, they were covered by a mask having a narrow slit across the middle of each of two chosen adjacent mirrors. The high-voltage bias setting of one of these mirrors was then adjusted to shift the white light fringe over to the center of the image as marked by the sharpness slit. This procedure was repeated for each pair of adjacent mirrors; the adjustments needed were typically a wavelength of light.

III. TEST RESULTS WITH ARTIFICIAL STARS

To test the ability of the telescope to compensate for atmospheric turbulence, we placed a neon-helium laser and an incandescent white-light source 250 meters from the laboratory window. The light from these "artificial stars" travelled along a horizontal path which bridged a canyon; this test range had a variety of seeing conditions depending on the weather, and provided a good simulation of observatory conditions

except for scintillation (the amplitude variations that are perceived as twinkling). Computer simulations[1] have shown that our ability to restore diffraction-limited imaging should be insensitive to the existence of scintillation.

To protect the photomultipliers from the full laser intensity, neutral density filters were placed in the optical path, typically introducing 10^4 in attenuation. Figure 6 shows the image of the laser as recorded by the scanning photomultiplier, both with and without the image-sharpening feedback. Comparison with a Monte Carlo calculation (dotted line) shows that the system is performing as expected. The small bumps near ± 2.5 arc sec are the innermost of a series of secondary maxima (several are visible in the figure) caused by the regularly spaced gaps between the six moveable mirrors. Computer simulations show that the light between the innermost bumps and the main diffraction peak is about half due to secondary maxima from a perfect diffraction pattern for this system, and half due to residual error in correcting the incident wavefront phase. The residual error arises from the use of six individual pistons instead of a smoothly deformable mirror. Figure 6 was made using mirror perturbations of 1/7 wavelength. We found, however, that the corrected diffraction pattern changed very little for perturbations varying from 1/20 to 1/5 wavelength. On the other hand, perturbations larger than 1/5 wavelength caused a noticeable increase to the light in the wings of the diffraction pattern, at the expense of the central maximum. This is as one would expect, since a coarse-grained correction of the mirrors leaves large residual phase errors, which in turn degrade the quality of the image.

To determine the least correctable brightness of objects, we placed

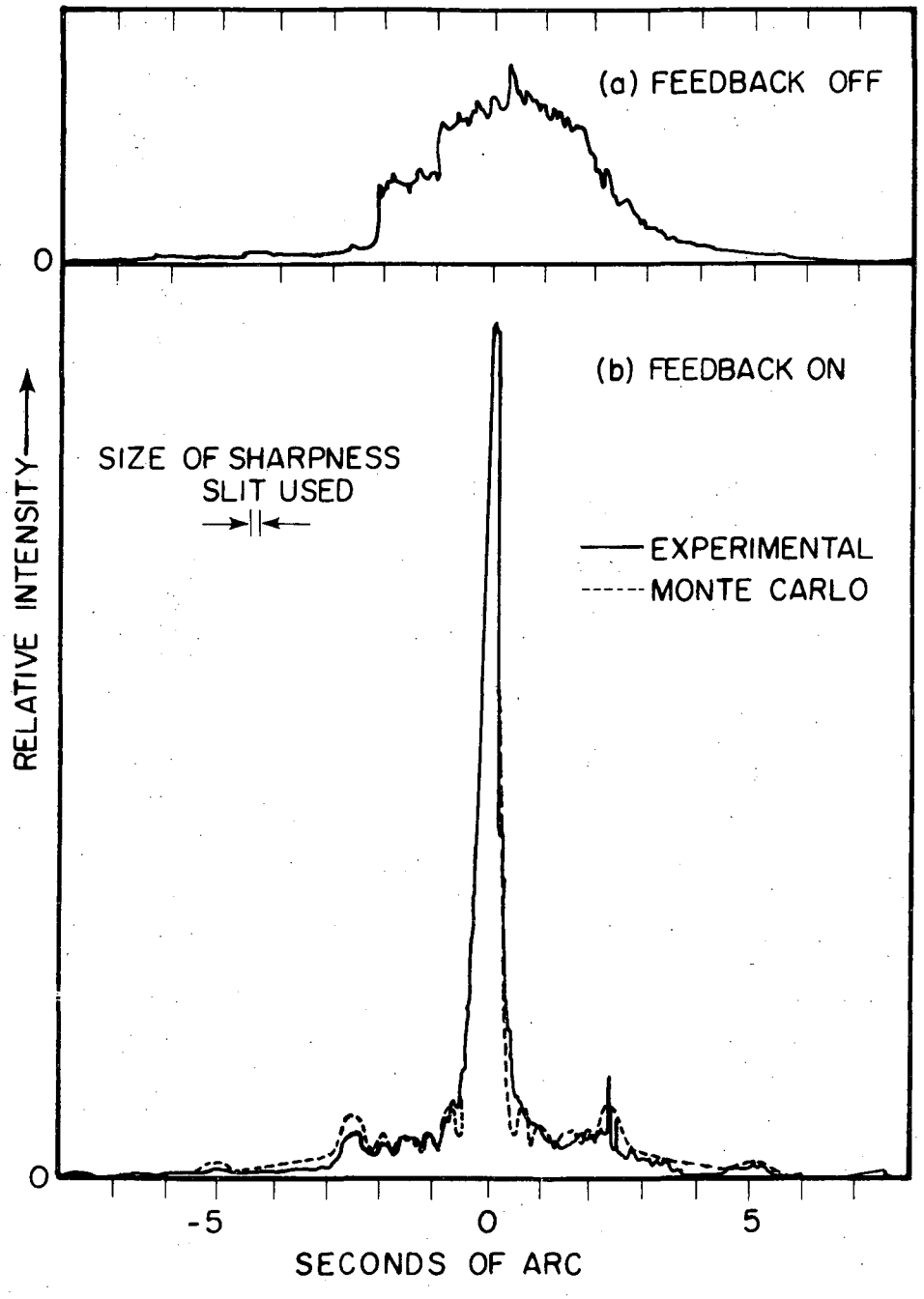

XBL 762-2228

Figure 6. Images of laser light viewed through 250 m of turbulent atmosphere. The agreement between corrected image and Monte Carlo calculation is good, and the corrected central diffraction peak is nearly a decade improved over the uncorrected image. The curves are normalized to the same area.

additional neutral-density filters in the optical path and observed the resulting image degradation. Using the visible bandpass relation between astronomical magnitude m and brightness B,

$$B = (4 \times 10^6)10^{-m/2.5} \quad \text{photons/cm}^2\text{sec} \qquad (3)$$

the laser corresponded to a magnitude -12 object. The laser image showed stabilization and good image quality until the light had been attenuated by a total factor of 5×10^6. This light level corresponds to about 100 photoelectrons in PM-1 for each integration time of 0.44 ms, which is close to the predicted 36 photoelectrons for a six-mirror system given by the simple analysis in ref. 1. At these low light levels, significant noise was contributed by photomultiplier dark-current, as well as photoelectron fluctuations. Figure 7 shows the deterioration of the image at low light levels, as a function of the numbers of photoelectrons produced by the image during one integration time. The numbers of photoelectrons given in this figure were obtained through a calibration of PM-1 with a light source of known intensity.

To get a quantitative measure of the time structure of the seeing, we turned off the feedback and analyzed the PM-1 output I(t) with a Hewlett-Packard Correlator Model 3721A to determine the integral

$$A(\tau) = \int_0^T dt\ I(t)\cdot I(t+\tau) \qquad (4)$$

where $T >> \tau$ and A(0) is normalized to unity. Figure 8 presents typical measurements of $A(\tau)$ with various seeing conditions. Image restoration was not generally possible when the characteristic coherence time of the seeing (defined to be that value of τ for which $A(\tau) = 0.5$) was shorter than the time for three passes through the mirrors. For the results presented here a single pass through the mirrors took about 4 msec. Local

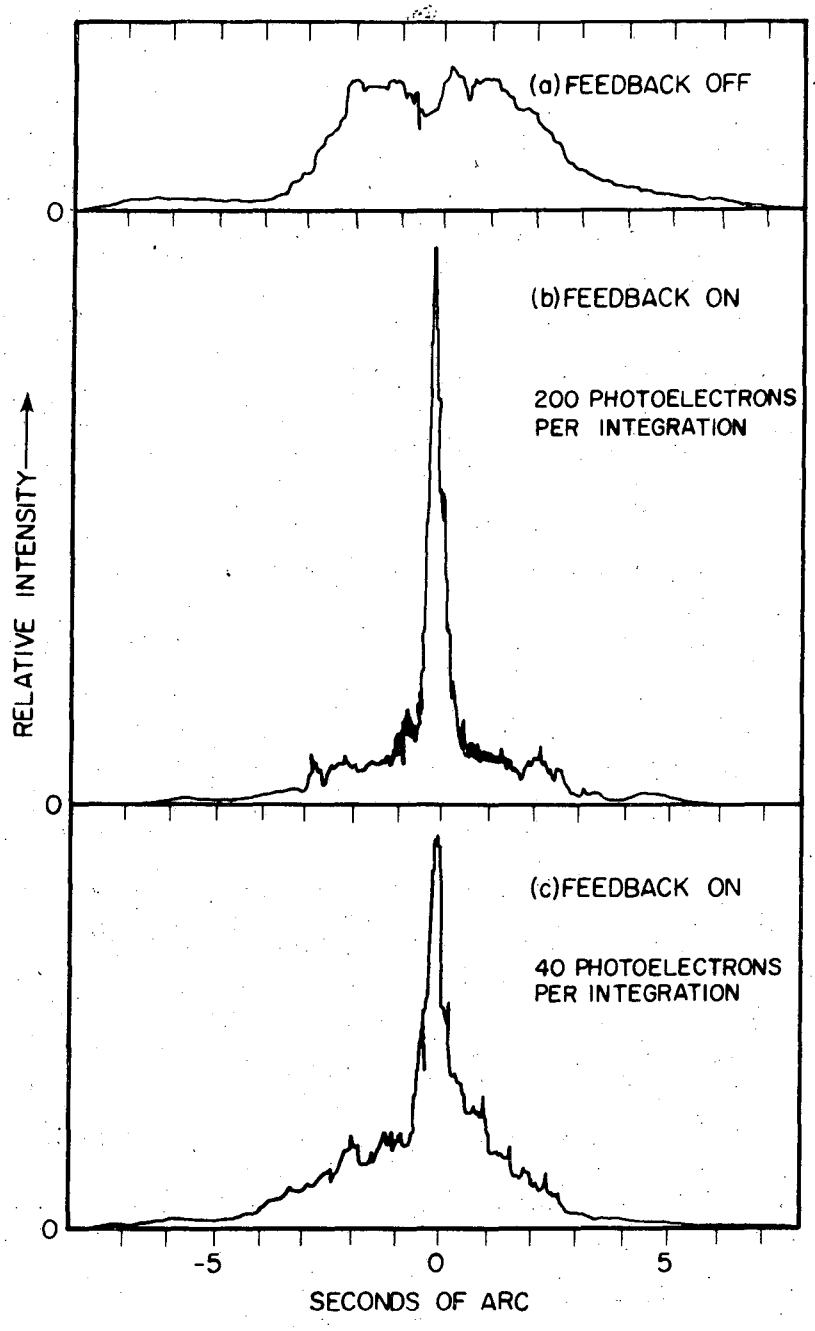

XBL 762-2229

Figure 7. Determination of dimmest correctable objects. The conditions are similar to those of figure 6, except neutral-density filters have been placed in the optical path to reduce the amount of light. The image quality in (b) is nearly as good as that of figure 6 even though the amount of light has been reduced by 100 times. However, the image quality degraded when the light was reduced in (c) to a level close to $N^2 = 36$ (N being the number of moveable mirrors) where theory predicts that degradation should set in. Curve (b) has a somewhat smaller normalization than curves (a) and (c).

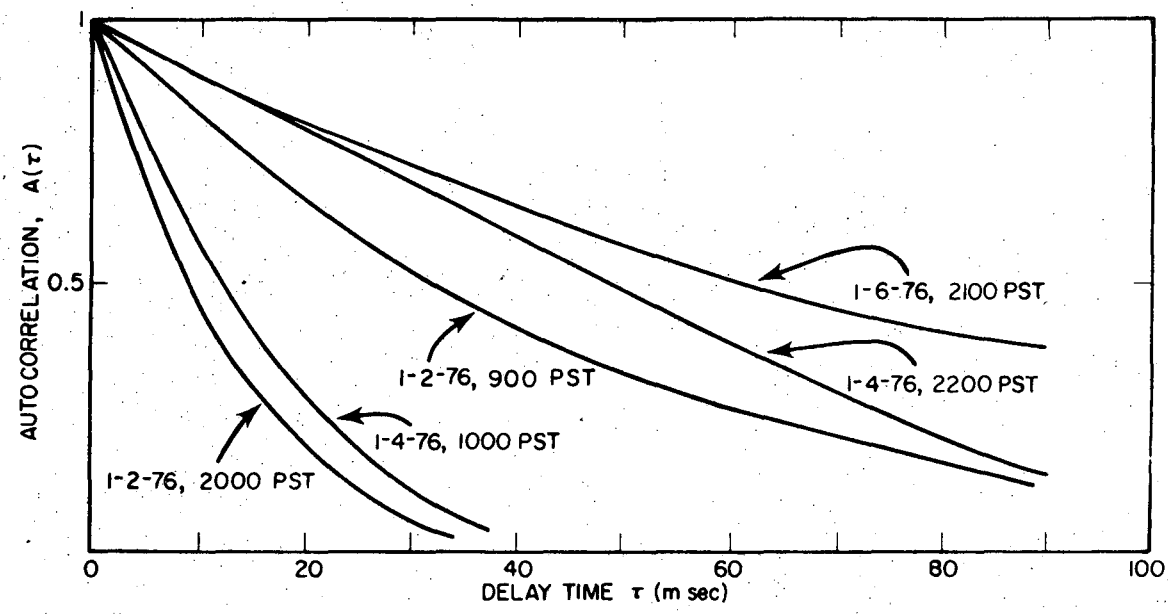

XBL 762-2230

Figure 8. Measurements of the autocorrelation function $A(\tau)$. These curves show the characteristic coherence time for speckles from the uncorrected laser image drifting and changing at the sharpness slit. The curves chosen represent a typical range of seeing experienced at our laboratory, with a high-quality window installed to isolate the work area from the outside. These curves illustrate the wide range of conditons that can occur within a relatively short time period.

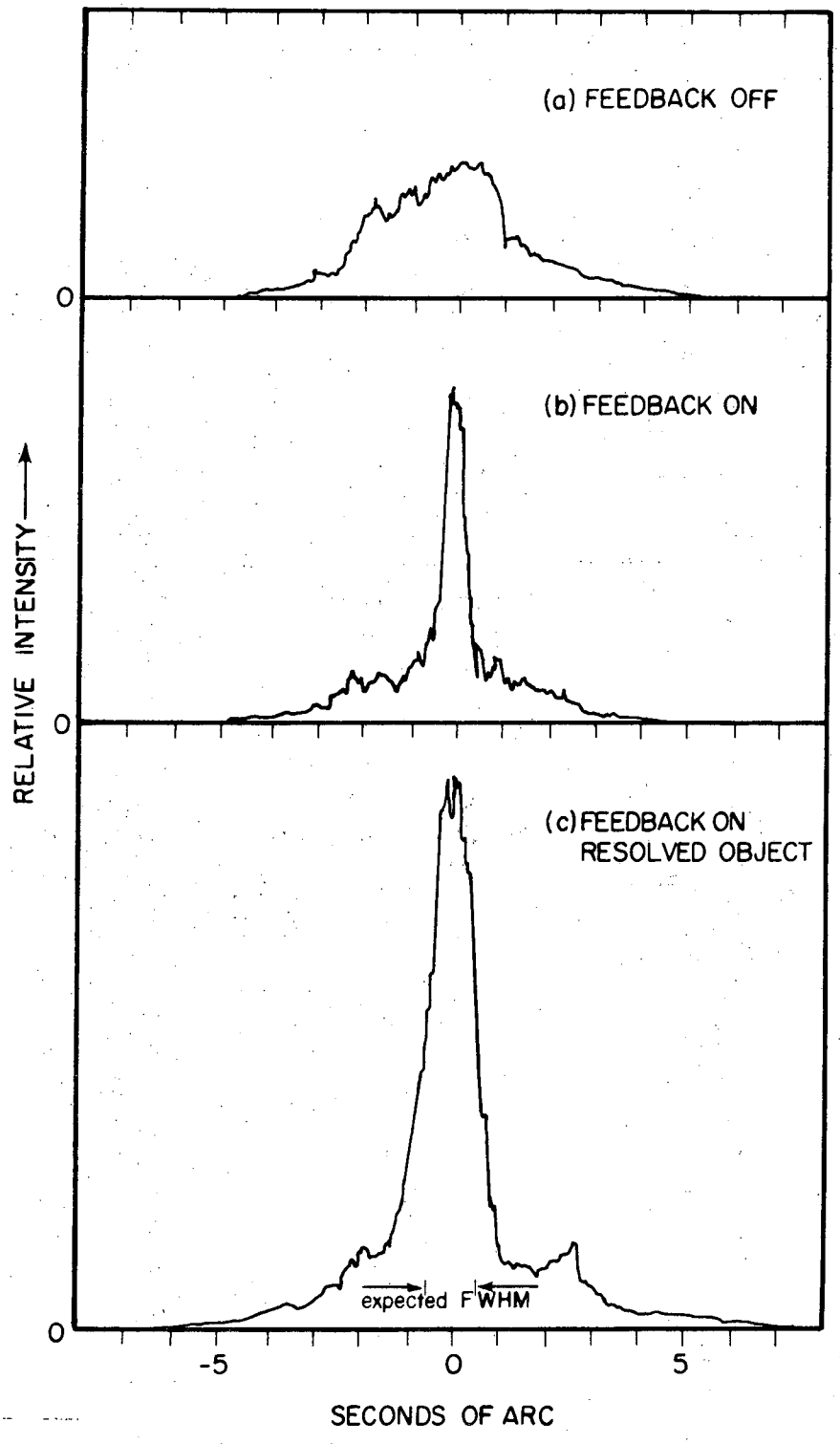

XBL 762-2231

Figure 9. White light images. An incandescent bulb with a 1 mm filament was placed 250 m from the telescope. In (a) and (b) a narrow mask was placed in front of the bulb to make an unresolvable object. In (c) the slit was removed to make a resolvable object with the expected FWHM as shown.

turbulence at the window of the room caused short coherence times, and the seeing was rarely correctable until an optical-quality glass window was put in place. With this improvement, correctable seeing conditions occurred about half the time.

We also tested the image-sharpening system on a white-light source. An incandescent bulb with a filament one millimeter in diameter was masked to 1/8 mm in apparent size in order to test fully the resolving capability of the telescope. Figure 9a shows the uncorrected image, and 9b the image with the feedback on. As with the laser, the system yielded an essentially diffraction-limited image. In order to test the system on an extended source, we removed the mask from the bulb; the resulting image is shown in figure 9c.

An interesting phenomenon arose in recording figure 9c. The expected diffraction-limited image of the helical filament, as viewed in our one-dimensional system, is substantially broader than the sharpness slit we used. As a result the image "rattled around" the slit, giving an image considerably broader than that expected. To alleviate this difficulty, we removed the steering and biased the pointing of the telescope, causing the slit to favor one edge of the image. The result has the expected FWHM, but is asymmetric, and has a spurious bump at 2 arc sec. These problems should not arise when we use a mask function $M(x,y)$ which is a closer match to the expected image.

IV. SUMMARY AND CONCLUSIONS

We have constructed and operated an image-sharpening system similar to that proposed in ref. 1, and have achieved essentially diffraction-limited performance from a 30 cm x 5 cm aperture when imaging both laser and white-light objects through 250 meters of turbulent atmosphere. The behavior of this system was accurately predicted by computer simulations. The telescope operated successfully for objects as dim as 5th magnitude, near the anticipated limit set by statistical fluctuations in the number of photoelectrons detected during each integration period. If the coherence time on good nights at observatories is as long as 50 ms, the integration time could be increased approximately ten-fold, thus allowing significant image sharpening for stars 7th magnitude or brighter. The design of the apparatus is such that it can conveniently be moved to an observatory and mounted on an equatorial drive without major disassembly or recalibration. In the near future we expect to report on tests made with astronomical objects.

ACKNOWLEDGEMENTS

This work was supported by the Energy Research and Development Administration, and by the National Aeronautics and Space Administration (grant NGR-05-003-553). We have received numerous helpful suggestions from D.D. Cudaback, L.V. Kuhe, and C.D. Orth. We are particularly grateful for the continuing encouragement and support given to this project by R.W. Birge and L.W. Alvarez.

REFERENCES

1. R.A. Muller and A. Buffington, J. Opt. Soc. Am. 64, 1200 (1974).

2. H.W. Babcock, Publ. Astron. Soc. Pac. 65, 229 (1953); H.W. Babcock, J. Opt. Soc. Am. 48, 500 (1958).

3. Partial descriptions of these systems may be found in the Digests of Technical Papers for the Topical Meeting on Optical Propagation Turbulence, July 9-11, 1974, Boulder, Colorado, and also for the Topical Meeting on Imaging in Astronomy, June 18-21, 1975, Cambridge, Massachusetts, both sponsored by the Optical Society of America. Additional details (including some further details of this work) will be presented at the S.P.I.E./S.P.S.E. Technical Symposium East, vol. 75, March 22-23, 1976.

4. F.J. Dyson, J. Opt. Soc. Am. 65, 551 (1975).

5. J.L. Gumnick and C.D. Hollish, IEEE Transactions on Nuclear Science 13, 72 (1966).

TECHNICAL INFORMATION DIVISION
LAWRENCE BERKELEY LABORATORY
UNIVERSITY OF CALIFORNIA
BERKELEY, CALIFORNIA 94720